Bulletin of Mathematical Biology Vol. 53, No. 5, pp. 701–719, 1991.
Printed in Great Britain.

0092-8240/91$3.00+0.00
Pergamon Press plc

BIFURCATING SPATIALLY HETEROGENEOUS SOLUTIONS IN A CHEMOTAXIS MODEL FOR BIOLOGICAL PATTERN GENERATION

■ P. K. MAINI*
Department of Mathematics,
University of Utah,
Salt Lake City, UT 84112, U.S.A.
■ M. R. MYERSCOUGH
School of Mathematics and Statistics,
University of Sydney,
Sydney, N.S.W. 2006, Australia
■ K. H. WINTERS
Theoretical Studies Department,
Harwell Laboratory,
Didcot, OX11 0RA, U.K.
■ J. D. MURRAY
Applied Mathematics,
University of Washington,
Seattle, WA 98195, U.S.A.

We consider a simple cell–chemotaxis model for spatial pattern formation on two-dimensional domains proposed by Oster and Murray (1989, *J. exp. Zool.* **251**, 186–202). We determine finite-amplitude, steady-state, spatially heterogeneous solutions and study the effect of domain growth on the resulting patterns. We also investigate in-depth bifurcating solutions as the chemotactic parameter varies. This numerical study shows that this deceptively simple–chemotaxis model can produce a surprisingly rich spectrum of complex spatial patterns.

1. Introduction. During the development of an embryo there is rapid growth, not only in cell numbers, but also in specialization and complex organization among cells. Cells in the vertebrate embryo divide, migrate, differentiate and form the various organs in the body. Many of these structures have a regular pattern, such as the vertebrae in the spine, the pattern of feather and scale

* Present address: Centre for Mathematical Biology, Mathematical Institute, 24–29 St. Giles', Oxford, OX1 3LB, U.K.

follicles on the integument and the branching structures of the neural and circulatory systems. The often striking pigment patterns on the integument of many vertebrates are generally formed during relatively early embryonic development. For example, in the case of the zebra with a gestation of about 360 days the stripe pattern is probably laid down by the fourth week.

Pigment patterns are generated by chromatophore cells which lie in the dermal or epidermal layers of the skin. There are several types of chromatophores each containing different pigments; the most common are melanin-bearing cells, melanophores, which contain black, brown or yellow pigments. Other types of pigment cells, for example xanthophores (orange and red pigments) and iridophores (which cause iridescent effects), are found in non-mammalian vertebrates. During development pigment cell precursors—chromatoblasts—originate in the neural crest. This tissue lies along the midline of the developing embryo and is formed by the edges of the neural plate as they fuse to form the neural tube. These cells spread over the skin at a roughly uniform density. Whether or not the skin develops a pigmented patch depends on whether pigment cells produce pigment or remain quiescent. Chromatophore interactions may result in pigmented cells and unpigmented cells gathering in different regions to produce stripes or spots (for example, Bagnara and Hadley, 1973). In the case of alligator stripes it appears that melanophores are present in the unpigmented regions but do not produce melanin (Murray *et al.*, 1990). Cells which are committed to pigmentation production are also able to divide for some time at least, although they may lose this ability later (Mayer, 1980). Pigment granules may be secreted into other cells in skin, hair or feathers producing pigmentation in these organs. Thus cell migration and cell differentiation are the two basic processes involved in the generation of pigmentation patterns of the vertebrate integument.

The principle mathematical models for pigmentation to date have been mainly reaction–diffusion models (Murray, 1979, 1981a,b; Bard, 1981). These models hypothesize the existence of chemicals (morphogens) which react and diffuse and, under appropriate conditions, generate spatially heterogeneous patterns. This chemical landscape is viewed as a pre-pattern to which cells then respond in some genetically pre-determined way and differentiate accordingly. This is the basis of positional information (Wolpert, 1969, 1981), whereby a spatially heterogeneous chemical concentration landscape can be transformed into a spatial pattern of differentiated cells. Such models have been very successful in producing patterns observed in animal coat markings and butterfly wings (Murray, 1981a,b), but the evidence for the existence of such morphogens is still the source of considerable controversy. A cellular automata model was proposed by Cocho *et al.* (1987a,b). This type of model can produce a variety of spatial patterns but these depend intimately on the assumed rules which govern the automata as well as the initial conditions. A major problem

with all automata models is the difficulty of relating the biology to the assumed rules. A different type of model, based on cell stimulation by the nervous system, has been proposed by Ermentrout *et al.* (1986) for shell patterns. This model is not appropriate for the situation we discuss here. The relatively new continuum mechanochemical theory (for a review see Murray *et al.*, 1988; Murray, 1989) of biological pattern formation can also generate similar patterns to those created by reaction diffusion models and their solutions exhibit similar developmental geometric constraints as described by Murray (1981b) and Oster and Murray (1989). Here, however, the patterns are in cell density, tissue deformation and tissue matrix density. In the development of pigmentation tissue deformation is clearly not a relevant consideration and so we need to look at alternative models if we wish to consider the movement of real biological cells which we believe to be the precursors of melanophores.

Recently, Oster and Murray (1989) proposed a simple cell–chemotaxis model for pattern formation which takes account of cell motility and chemotaxis, the chemical process by which cells migrate up a chemical gradient. In this paper we consider this chemotactic mechanism for pattern formation and propose it as a candidate mechanism for chromatoblast patterning in the integument. With this model chromatoblasts both produce and respond to the chemoattractant. Such a mechanism would promote localization of differentiated cells in certain regions of the skin such as spots or stripes. Le Douarin (1982) speculated that chemotaxis may be a factor in the localization of pigmented cells in the skin. Cocho *et al.* (1987b) suggested that such a mechanism might operate in the rounding up of pigment spots. The model we study here has also been proposed by Murray (1988) and Murray *et al.* (1990) for the stripe and shadow patterns on the alligator (*Alligator mississipiensis*). Among other things their experimental results unequivocably show that scale is crucial in determining the number of stripes on alligators. They also found higher densities of melanocytes in the dark melanin stripe regions. The same model has also been shown to generate many of the dramatic patterns found on snakes (Murray and Myerscough, 1990).

In Section 2 we briefly describe the chemotaxis model. A linear analysis, sequestered in the Appendix, indicates its pattern generation capability. In many developmental situations the spatial organization of pattern takes place on a time scale commensurate with significant growth of the embryo (Murray *et al.*, 1990). Accordingly it is of considerable interest to investigate the effect of such growth on the detailed patterns which might be created. One of the main purposes of this study is to investigate this by considering the domain dimensions to be extra parameters in the model mechanism. We specifically consider here the bifurcation from one steady-state, spatially heterogeneous solution to another as we vary the linear dimension of the

domain. Also, it is possible that the ultimate observed pattern on an animal is not the steady-state pattern generated by a model as $t \to \infty$ but rather an intermediate pattern locked in when cells cease, for example, to produce the chemoattractant.

In Section 3 we study these solution behaviours of the model on a rectangular domain using the package ENTWIFE and show that the model can exhibit an astonishingly wide range of spatially heterogeneous solutions which bifurcate off other patterned solutions as one or other of the parameters is varied: we mainly consider variation in the domain geometry and scale and the chemoattractant parameter. Many of the patterns do not seem to have been produced so far by other model mechanisms. Finally, in Section 4 we briefly discuss the results and their biological implications.

2. Cell–Chemotaxis Model. The model can be interpreted in terms of local activation and lateral inhibition (Oster and Murray, 1989) where the local activation, or aggregation, force on the pigment cells is chemotaxis—the directional movement of cells up a gradient in chemical concentration. Chemotaxis is a major factor in many developmental situations. There is clear evidence that at least three kinds of embryonic cells respond chemotactically *in vivo*, namely neuroblasts, leukocytes and endothelial cells (Trinkaus, 1984). The chemotactic response of the slime mold *Dictyostelium discoideum* to cyclic adenosine monophosphate (cAMP) is well known and has been extensively studied both theoretically (for example, Keller and Segel, 1970) and experimentally (for example, Newell, 1983). The seminal model mechanism of Keller and Segel (1970) was in fact the motivation for the Oster and Murray (1989) model, which is that studied in depth here.

The model mechanism involves the cell density, $n(\mathbf{x}, t)$, and chemoattractant concentration, $c(\mathbf{x}, t)$, where $\mathbf{x}$ and t are the spatial coordinate and time respectively, and consists of equations which describe their motion and net production. The general form of the cell equation is

$$\frac{\partial n}{\partial t} = -\nabla \cdot \mathbf{J}_n + R(n) \tag{1}$$

where $\mathbf{J}_n$ is the flux of cells and $R(n)$ the net cell production. We assume that there are two contributions to the flux term, namely random Fickian diffusion with $\mathbf{J}_{\text{diffusion}} = -D_n \nabla n$ where D_n is the diffusion coefficient, and chemotaxis where $\mathbf{J}_{\text{chemotaxis}} = \alpha n \nabla c$ where α is the chemotaxis coefficient. We take the cell production term to be adequately described by logistic growth of the form $R(n) = rn(N-n)$ where rN is the linear mitotic growth rate with r and N both non-negative constants. N is a measure of the total number of cells present. The

logistic growth term is the simplest way to describe the characteristic sigmoidal growth exhibited by several cell types. With these the equation for cell density is

$$\frac{\partial n}{\partial t} = \underset{\text{diffusion}}{D_n \nabla^2 n} - \underset{\text{chemotaxis}}{\alpha \nabla \cdot (n \nabla c)} + \underset{\text{mitosis}}{rn(N-n)}. \tag{2}$$

We assume the cell secretes its own chemoattractant in a Michaelis–Menten fashion, that it diffuses with diffusion coefficient D_c and degrades according to first order kinetics. The equation for the chemotactic concentration c is then

$$\frac{\partial c}{\partial t} = \underset{\text{diffusion}}{D_c \nabla^2 c} + \underset{\text{production}}{\frac{Sn}{(\beta + n)}} - \underset{\text{degradation}}{\gamma c} \tag{3}$$

where S, β and γ are positive constants.

We are interested in pattern formation on the integument of developing vertebrates so we consider these equations on a finite domain D with zero flux boundary conditions, namely

$$\mathbf{n} \cdot \nabla c = \mathbf{n} \cdot \nabla n = 0 \quad \text{for} \quad \mathbf{x} \in \partial D \tag{4}$$

where $\mathbf{n}$ is the unit outward normal to the boundary ∂D. Periodic boundary conditions are also biologically relevant. The mathematical formulation of the model consists of equations (2) and (3) with boundary conditions (4). In equations (2) and (3) we have taken the simplest, yet biologically reasonable, forms for the non-linear source/sink terms. We would expect more complex forms of these functions to lead to yet more diverse pattern forming ability of this mechanism.

We first write the model in non-dimensional terms which reduces the number of parameters, by introducing

$$\mathbf{x}^* = \left[\frac{\gamma}{D_c s}\right]^{1/2} \mathbf{x}, \quad t^* = \frac{\gamma t}{s}, \quad n^* = \frac{n}{\beta}, \quad c^* = \frac{\gamma c}{S}$$

$$N^* = \frac{N}{\beta}, \quad D^* = \frac{D_n}{D_c}, \quad \alpha^* = \frac{\alpha S}{\gamma D_c}, \quad r^* = \frac{r\beta}{\gamma} \tag{5}$$

where the dimensionless s is a scale factor: we can think of $s=1$ as the unit domain and carry out the computation on a fixed domain size and increase s to simulate a larger domain. This procedure was used extensively in reaction diffusion simulations by Murray (1979, 1981a,b). With equations (5) the non-

dimensional equations become, on omitting the asterisks for notational simplicity,

$$\frac{\partial n}{\partial t} = D\nabla^2 n - \alpha\nabla \cdot (n\nabla c) + srn(N-n) \tag{6}$$

$$\frac{\partial c}{\partial t} = \nabla^2 c + s\left(\frac{n}{1+n} - c\right) \tag{7}$$

$$\mathbf{n} \cdot \nabla c = \mathbf{n} \cdot \nabla n = 0, \quad \mathbf{x} \in \partial D \tag{8}$$

where ∂D is now the boundary of the scaled domain.

In the subsequent analysis we consider the domain D to be rectangular and use Cartesian coordinates, so $\mathbf{x} = (x, y)$.

The system (6), (7) and (8) has two uniform steady-states: $(n, c) = (0, 0)$ and $(N, N/(1+N))$. A linear analysis about these uniform states shows that (0, 0) is always unstable while in certain parameter regimes the non-trivial solution can be driven unstable by spatially heterogeneous perturbations and evolve to inhomogeneous spatial patterns in n and c. This is the usual way spatial patterns are generated in most models for biological pattern formation (see, for example, Murray, 1989). The nature of the pattern is governed by the non-dimensional parameter set (D, α, r, N, s) and the size and shape of the domain. By suitable choice of the parameter set a particular pattern may be selected to give a mode (m, l) for integers m and l where the spatial eigenfunction of the linearized system which satisfies the boundary conditions (8) is proportional to $\cos m\pi x/L_x \cos l\pi y/L_y$ where L_x and L_y are the length and breadth of the rectangular domain respectively. For example, a pattern of lateral stripes is given by the $(0, l)$ mode where the higher the value of l the more stripes we have on the domain. In order to select a mode (m, l) on a rectangular domain we require (see the Appendix for details)

$$\frac{rNs^2}{D} = \pi^4 \left\{\frac{m^2}{L_x^2} + \frac{l^2}{L_y^2}\right\}^2 \tag{9}$$

$$\left[rN + D - \frac{N\alpha}{(1+N)^2}\right]^2 = 4rDN. \tag{10}$$

3. Two-dimensional Steady-state Patterns. The analysis of the last section, detailed in the Appendix, suggests that system (6)–(8) can evolve from an initial non-trivial uniform steady-state to a spatially patterned steady-state in cell density n and chemoattractant concentration c. In this section we investigate possible steady-states using the software package ENTWIFE, which solves

non-linear steady-state problems by discretization in the finite-element approximation using a standard Galerkin formulation (Winters, 1985). The package locates the critical value of a chosen parameter for which the uniform steady-state bifurcates to a non-uniform steady-state and follows this solution as the bifurcation parameter changes (Winters, 1987). We present results of a detailed numerical simulation obtained by using ENTWIFE. The numerical and analytical details will be reported elsewhere (Winters *et al.*, 1991). In this paper we simply concentrate on the different types of patterns exhibited. The non-dimensionalized steady-state problem is, from equations (6)–(8),

$$D\nabla^2 n - \alpha\nabla\cdot(n\nabla c) + srn(N-n) = 0 \tag{11}$$

$$\nabla^2 c + s\left[\frac{n}{1+n} - c\right] = 0 \tag{12}$$

$$\mathbf{n}\cdot\nabla c = \mathbf{n}\cdot\nabla n = 0, \quad \mathbf{x}\in\partial D. \tag{13}$$

There are three main ways in which pattern can be generated and we discuss each in turn.

(a) *Mode isolation.* In the Appendix we show that the dispersion relation for the full linearized system of evolution equations indicates bifurcation to spatial instability at the wavenumber $s[rN/D]^{1/2}$ for a critical α given by equation (A5b) in the Appendix. With zero flux boundary conditions on a 1×4 domain, this will be an admissible mode if

$$\frac{rNs^2}{D} = \left(m^2\pi^2 + \frac{l^2\pi^2}{16}\right)^2 \tag{14}$$

where m and l are non-negative integers which are not zero simultaneously. At this wavenumber the dispersion is zero and we have a solution to the steady-state problem (11)–(13) which will be non-uniform if equation (14) holds for some m and l. By choosing r, N, s and D appropriately [and the corresponding α from equation (A5b)] we can isolate a particular mode (m, l); see Fig. 1. In such (r, N, s, D) parameter space, ENTWIFE can find the critical bifurcation value for α and solve equations (11)–(13) as α increases (supercritical) or decreases (subcritical) from this value. Figure 2 illustrates typical solutions.

(b) *Continuous variation of a single parameter.* From equation (A5) it is clear that by appropriately varying any one of the five parameters r, N, s, D or α, the uniform steady-state can evolve to a non-uniform steady-state (see Fig. 1). The chemotaxis parameter α is a key parameter so we fix the others and use ENTWIFE to locate bifurcations in α and to follow the corresponding

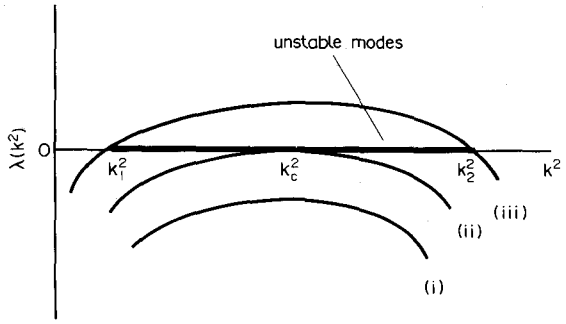

Figure 1. Variation of dispersion relation $\lambda(k^2)$ from equation (A3) as α increases for fixed N, r, D and s. In the appropriate parameter domain, if $\alpha<\alpha_c$ [given by equation (A5b)] the dispersion relation is as illustrated in (i) and the uniform solution $(N, N/(1+N))$ persists. (ii) At $\alpha=\alpha_c$, wavenumber $k_c^2=s(rN/D)^{1/2}$ is neutrally stable. For $\alpha=\alpha_c+\varepsilon$, $0<\varepsilon\ll 1$ a non-uniform solution to the steady-state problem (11)–(13) exists if k_c is a permissible wave number [that is, the mode with wavenumber k_c satisfies the boundary conditions (13)]. (iii) $\alpha>\alpha_c$. As α increases past α_c, the zeros of the dispersion relation separate (k_1 and k_2). If one of them passes through a permissible wavenumber, that mode is a solution to the steady-state problem and is located by ENTWIFE.

solutions. This results in a state diagram which illustrates how the patterns vary with changing α. Figure 3 shows part of this diagram. Several important points arise here.

(i) The branch for mode (0, 2) heads back to the uniform steady state via a secondary bifurcation on the (0, 4) branch.

(ii) On several branches, for example (0, 3), (1, 1) and (1, 2), the peaks of cell density sharpen as α increases. This is typical of chemotactic-type systems because of the self-enhancing feature of the aggregation process. In our system, however, chemotactic collapse, the phenomenon whereby the system evolves to a Delta function in the chemotactically responding cell population, is not possible with the logistic growth term.

(iii) In some cases peaks moved and split as shown in Fig. 4.

It is possible to move off a branch by varying a second parameter. Preliminary investigations using the scale factor s as the secondary parameter show that in many cases the behaviour of the solution does not change qualitatively unless, of course, s varies significantly [see (c), (ii) below].

(c) *Domain scale and geometry.* These are very important factors in controlling pattern formation as they are in most pattern generation mechanisms (see the review in Murray, 1989). With the domain we consider here there are two important roles they can play.

(i) Separation of degenerate modes. For example, on a 1×4 domain, modes (1, 0) and (0, 4) branch off at the same parameter values. However, if we change

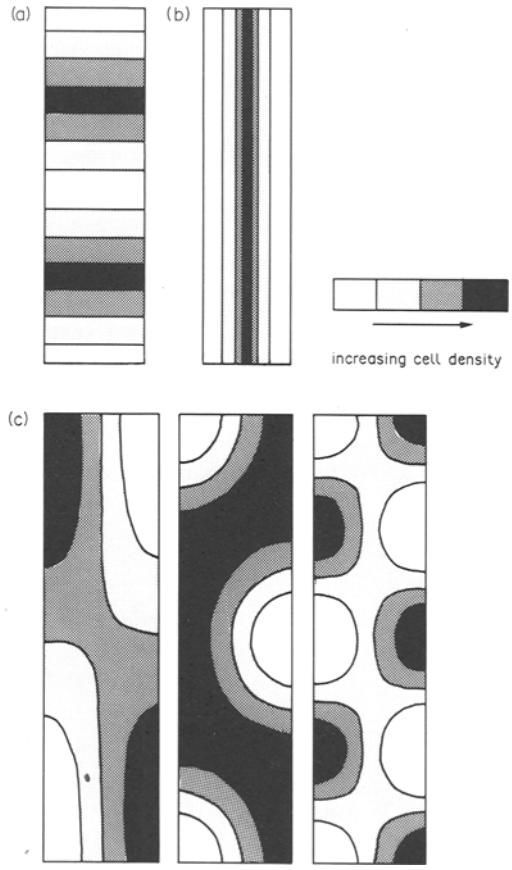

Figure 2. Solutions to equations (6)–(8) using mode selection. In each case we show only the cell density n. The chemoattractant concentration, c, is qualitatively similar in behaviour. (a) Mode (0, 4), parameter values $r=24.4$, $\alpha=118.68$. (b) Mode (2, 0), parameter values $r=389.6$, $\alpha=1782.0$. (c), (i) Mode (1, 1), $r=28.22$, $\alpha=135.16$. (ii) Mode (1, 2), $r=38.05$, $\alpha=175.76$. (iii) Mode (1, 4), parameter values $r=1.52$, $\alpha=27.06$. Note that on a 1×4 domain the modes in (a) and (b) are degenerate in that for (a) mode (1, 0) is also a solution while for (b) (0, 8) is also a solution. However, we can separate such degenerate modes by changing the domain slightly so that for each case only one mode will satisfy the boundary conditions. In (a) we took the domain as 1.1×4 while in (b) the domain was 1×4.1. In all the above simulations, $N=1$, $D=0.25$, $s=1$.

the domain to 1.1×4 and keep the parameters fixed, then only (0, 4) will branch off, as it is the appropriate mode for the boundary conditions (see Fig. 2a). When we perturb the domain in the other direction, that is, make it 1×4.1, we obtain the (1, 0) mode (Fig. 2b).

(ii) By increasing the scale, that is increasing s, it is possible to enhance the richness of the patterns. Heuristically this is to be expected; we can think of this

as simply enabling more pattern to 'fit into' the domain (Fig. 5). The effect of varying scale via the width—the L_x—of course also affects the pattern as in Fig. 6.

As we noted in the case of alligator stripes, melanocytes were found in the unpigmented areas (Murray *et al.*, 1990) which suggests a threshold cell density before a melaninistic pattern appears. If a pattern appears at a different cell density threshold, that is other than simply at a density above the uniform steady-state N, we obtain different patterns: see Fig. 6. The variability in pattern as a result of varying the threshold was pointed out and used by Murray (1981b) to account for the similar but quantitatively different patterns observed on the integument of different giraffe species.

4. Discussion of Results. The development of structure and form is a key issue in embryology and is the source of much experimental and theoretical research. Mathematical models have had a significant influence in guiding and stimulating experimental programmes and play a major role in proposing candidate systems for the underlying mechanisms involved in pattern formation. Two major modelling approaches have been proposed, namely the well known reaction–diffusion models based on Turing's (1952) theory of morphogenesis [see the books by Meinhardt (1982) and Murray (1989)] and the Oster–Murray mechanochemical models [see the extensive discussion in Murray (1989)]. The mechanochemical approach proposes that the physico-chemical environment of the cell leads to a direct pattern of cell aggregations. Several other types of models have been proposed for pattern formation, for

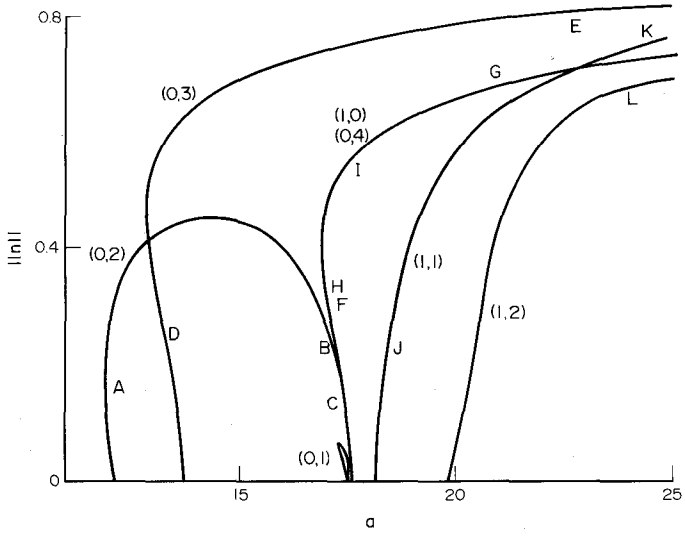

Figure 3(a).

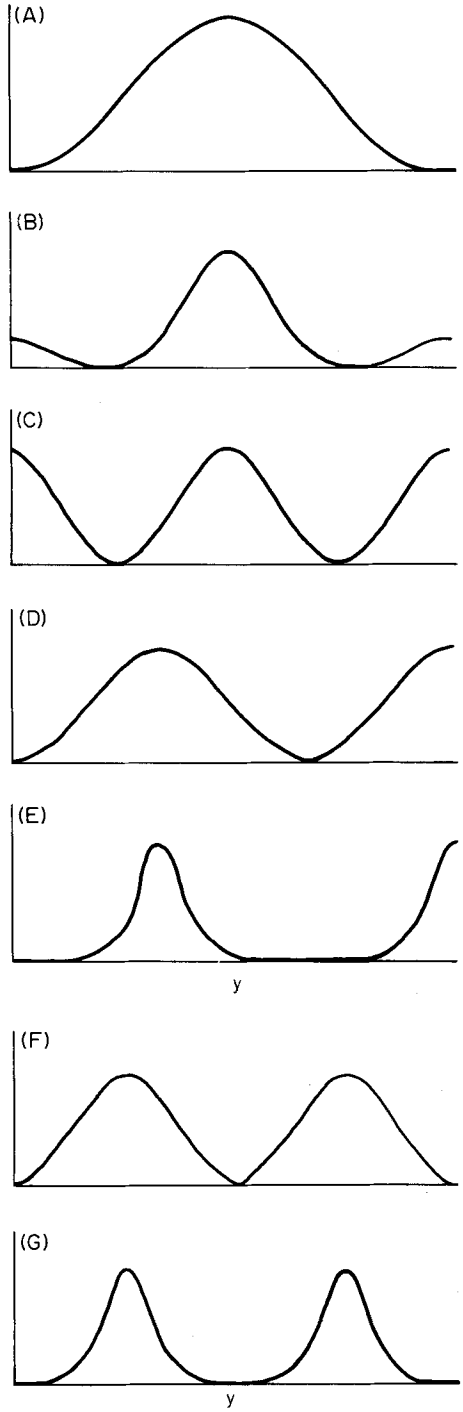

Figure 3(a) continued.

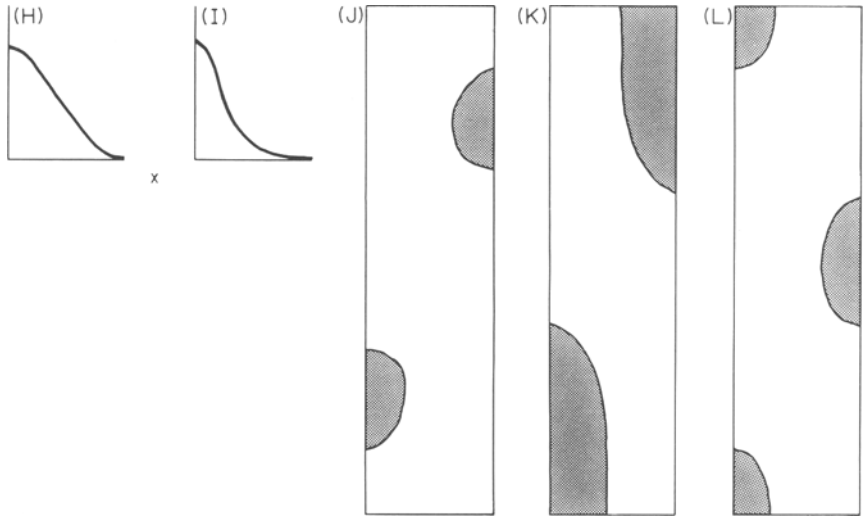

Figure 3(a) continued. (See caption with Figure 3(b).)

example cellular automata models, gradient models (Wolpert, 1969, 1981), and polar coordinate model (French *et al.*, 1976). Of these approaches, reaction–diffusion and cellular automata are the theories that have been proposed for animal coat markings (see Introduction).

The cell–chemotaxis model we consider here for animal coat markings falls into the mechanochemical group of models and has been applied to various biological situations, most recently to stripe initiation in alligators (Murray, 1988; Murray *et al.*, 1990) and pigmentation patterning on snakes (Murray and Myerscough, 1990). Analytically finite-amplitude, spatially structured, steady-state solutions in one-dimension of a simplified version of equations (2)–(4), wherein the mitosis term was set to zero, were recently considered by Grindrod *et al.* (1989).

In this paper we have presented a preliminary study of the pattern forming potential of a mechanochemical model, based on the chemotactic response of cells, as it might apply to animal skin patterns. Linear analysis presages the existence of spatially heterogeneous steady-state solutions to the model and the package ENTWIFE not only confirms this but also calculates steady-state solutions and shows how they behave as the bifurcation parameter changes. Although we restricted our study to patterns on a 1×4 domain, or small perturbations from it, and selected only a few of the possible types of pattern to consider, it is easy (but computationally expensive) to extend the study to other domains with a corresponding greater range of patterns. The preliminary results presented here, however, clearly show the remarkable wealth of possible spatially structured solutions that such a simple set of chemotactic equations can exhibit.

The model exhibits stripes, both longitudinal and lateral, and spots. Such

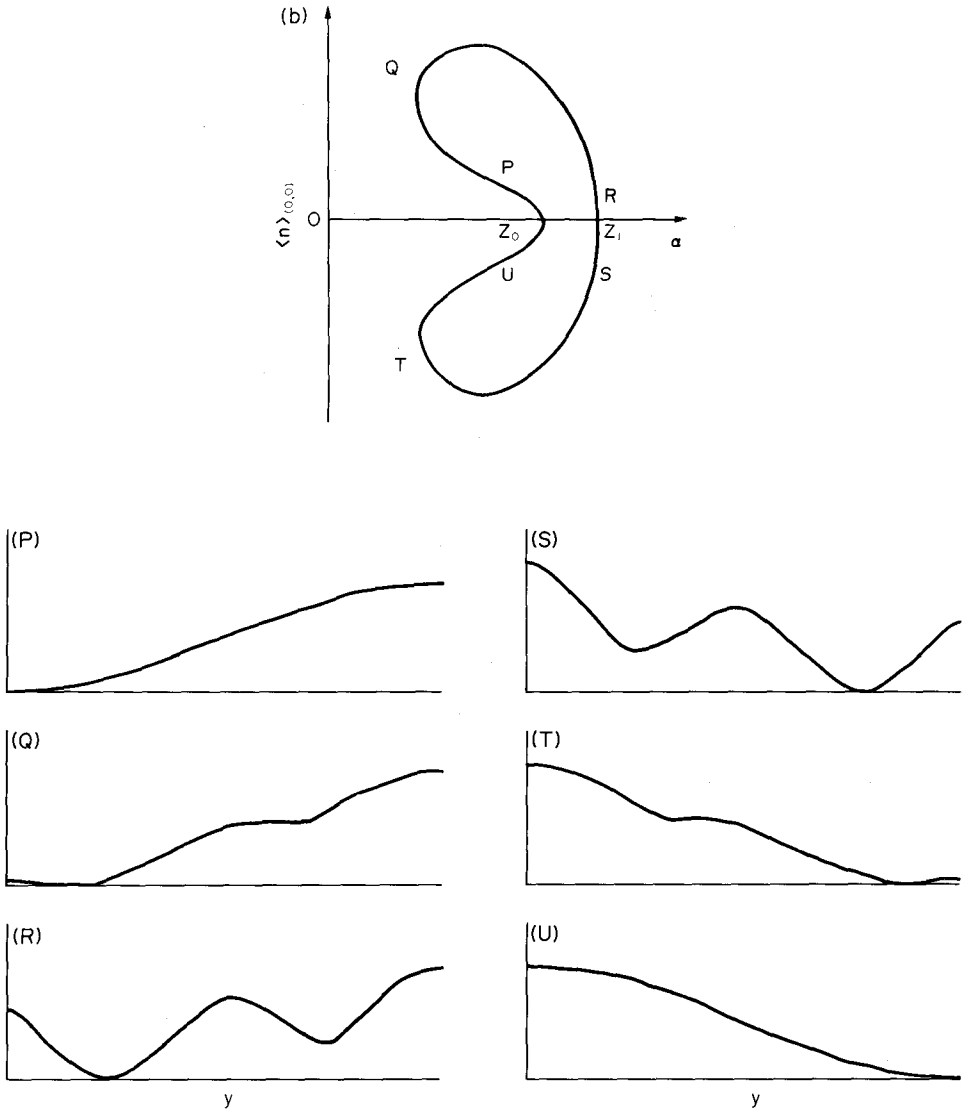

Figure 3(b).

Figure 3. (a) State diagram for fixed parameter values $r=1.52$, $N=1$, $s=1$, $D=0.25$ and varying α on 1×4 domain. Note that modes (0, 4) and (1, 0) are degenerate. $\|n\| = \int_D |N-n| dx dy / \int_D dx dy$, D = domain. The letters A–L on the state diagram denote the patterns indicated. (b) Magnified view of the bifurcation of mode (0, 1). A different choice of measure makes it clear that this is in fact a pitchfork bifurcation where the two branches of the pitchfork join on to each other. Z_0 is the bifurcation point, Z_1 is where the branch crosses the α axis without bifurcation. Letters P–U refer to the solutions illustrated and $\langle n \rangle_{(0,0)} = (n-N)$ evaluated at the point (0, 0). Note that the intersection of branches are overlaps and not secondary bifurcations, which were not considered in this study.

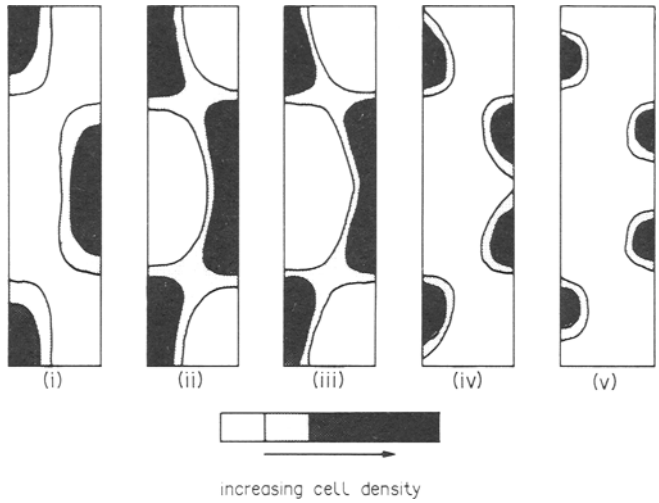

Figure 4. As α increases along branch (1, 2) of Fig. 3, the peaks of cell density move and one peak splits. (i) $\alpha = 23.75$, (ii) $\alpha = 27.59$, (iii) $\alpha = 32.71$, (iv) $\alpha = 42.95$, (v) $\alpha = 63.43$.

patterns are important from the viewpoint of animal coat markings. It is clear that increasing the domain size can increase the richness of pattern. Murray (1979, 1981a,b), in a series of papers, proposed a reaction–diffusion model as a candidate pre-pattern mechanism for melanoblast cells, which could then respond to the chemical pre-pattern in a genetically pre-determined fashion. However, the migration of the pigment cells from the neural crest and their strongly invasive properties suggest that perhaps a model based on cell motility may be more appropriate. The experimental results of Murray *et al.* (1990) lend support to this hypothesis.

Here, we have established that a cell–chemotaxis model can produce a wide variety of observed patterns. This is a necessary condition to be fulfilled by any model that purports to account for any developmental phenomenon. Of course it is not sufficient; each model should be able to make testable predictions. The section on mode isolation shows that the spacing of the patterns predicted by the model may vary by changing, for example, the mitotic rate of cells or total number of cells. Decreasing either causes the pattern spacing to increase or disappear altogether. This is a prediction of the model that should be tested experimentally. Similar predictions emerge from a mechanochemical approach, for example, to chondrogenesis and to feather germ formation. Treatment with a mitotic inhibitor reduced the number of digits in the salamander limb (Alberch and Gale, 1983; Oster *et al.*, 1988); while irradiation of the feather forming region of the chick, which reduced the total number of cells, increased the spacing of the feather primordia (D. Davidson, personal communication, 1984). The predictions of these mechanochemical models are

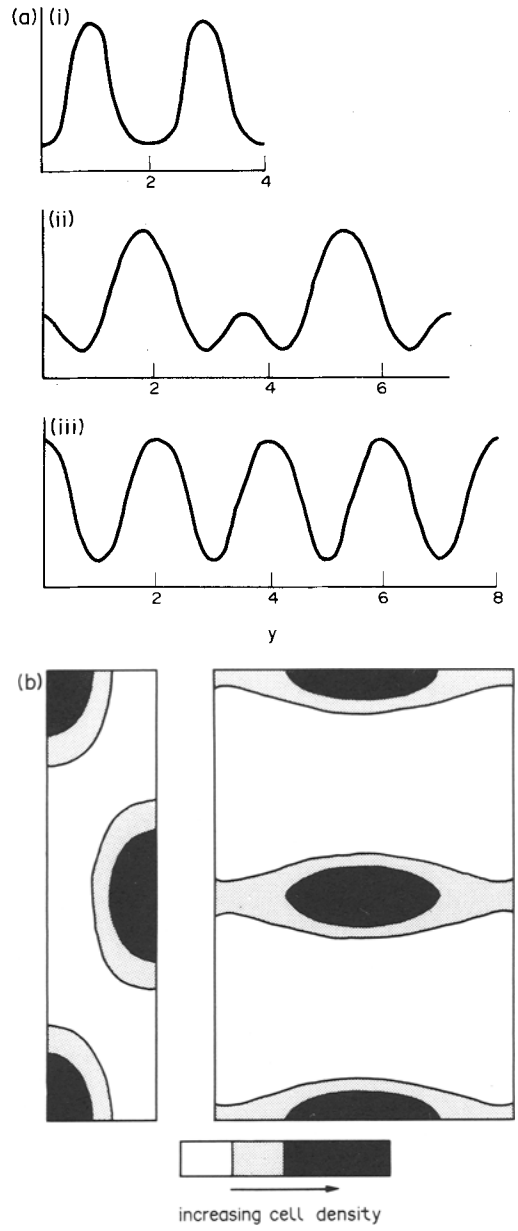

Figure 5. The effect on the solution of changing domain scale. In each case we show only the cell density n. The chemoattractant concentration, c, is qualitatively similar. (a) Parameter values $r=1.52$, $N=1$, $s=1$, $D=0.25$, $\alpha=17.57$. On a 1×4.1 domain the solution is a (0, 4) mode. If we continue along a solution branch with increasing scale in the y-direction, the solution changes to a (0, 8) mode on a 1×8.2 domain. (b) Parameter values $r=1.52$, $N=1$, $s=1$, $D=0.25$, $\alpha=20.5498$. On a 1×4 domain, the solution is a (1, 2) mode. As we continue along the solution branch with increasing scale in the x-direction, the solution changes to a (2, 2) type mode for domain 2.65×4.

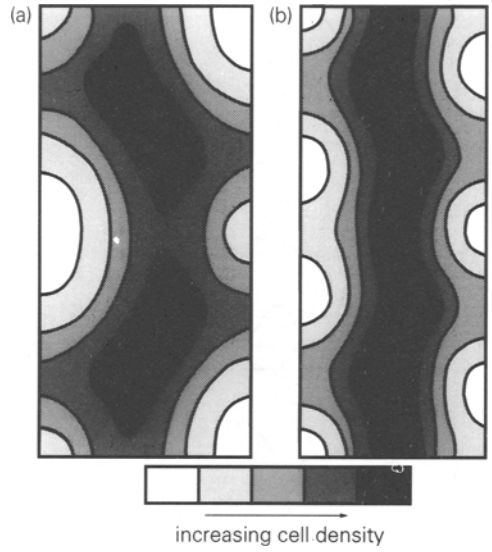

Figure 6. The effect of changing domain size in the x-direction for the (1, 4) mode. Note that by taking different threshold cell densities, we can generate different patterns. For example, in (b) if the threshold is at low cell density, this pattern is a series of semi-circular spots. However, if the threshold is at high cell density, the pattern is a wavy stripe.

easier to test than reaction–diffusion type models, where the predictions are in terms of properties of highly elusive morphogens. In the simulations presented, the stability of the patterns was not fully investigated. Thus some of these patterns may be unstable. However, in view of the fact that observed developmental patterns may be in response to transient underlying patterns, unstable patterns are still relevant. We note that a detailed eigenvalue analysis along every solution branch would be necessary to prove stability of each pattern and to discount possible Hopf bifurcation to time-periodic pattern. Such a detailed study is outside the scope of the present work.

Perhaps the most important result of this paper is to highlight the crucial importance of the effect of domain growth on the patterns formed. If the time it takes the pattern mechanism to generate pattern is commensurate with significant growth of the embryo then the final pattern can be very different if the mechanism operates on a fixed domain. Many of the observed animal integument patterns could be the result of mechanisms which have been operative on a growing domain.

This work (JDM) was supported in part by Grant DMS-9003339 from the U.S. National Science Foundation, and by the Underlying Programme of the U.K.A.E.A. P.K.M. and M.R.M. would like to thank U.K.A.E.A. Harwell for

their hospitality and support. M.R.M. would like to acknowledge an Overseas Research Studentship (ORS) Award from the British Government.

APPENDIX

Here we carry out the linear analysis of system (6)–(8). There are two uniform steady-states for (n, c) given by $(0, 0)$ and $(N, N/(1+N))$. The steady-state $(0, 0)$ is always unstable by inspection so we consider only the non-zero steady-state $(N, N/(1+N))$ here.

In the usual way we set $n=N+u$, $c=N/(1+N)+v$ where $|u|$, $|v|$ are small, substitute into (6)–(8) and retain only linear terms. This gives the linear equations, which govern behaviour near the steady-state, as

$$\frac{\partial u}{\partial t} = D\nabla^2 u - \alpha N\nabla^2 v - rNsu \tag{A1a}$$

$$\frac{\partial v}{\partial t} = \nabla^2 v + s\left[\frac{u}{(1+N)^2} - v\right] \tag{A1b}$$

$$\mathbf{n}\cdot\nabla u = \mathbf{n}\cdot\nabla v = 0, \quad \mathbf{x}\in\partial D. \tag{A1c}$$

We look for solutions to equations (A1) in the form

$$\begin{bmatrix} u \\ v \end{bmatrix} = \begin{bmatrix} u_0 \\ v_0 \end{bmatrix} \exp[i\mathbf{k}\cdot\mathbf{x} + \lambda t] \tag{A2}$$

where $\lambda = \lambda(k)$ determines the temporal growth rate of the disturbance with wave vector $\mathbf{k}$. Non-trivial solutions for u_0 and v_0 exist only if λ, the dispersion relation, satisfies the characteristic polynomial

$$\lambda^2 + [(D+1)k^2 + rN + s]\lambda + \left[Dk^4 + \left\{rNs + Ds - \frac{(sN\alpha)}{(1+N)^2}\right\}k^2 + rNs^2\right] = 0 \tag{A3}$$

and the wave with wavenumber $|\mathbf{k}|$ satisfies the boundary conditions (A1c). If $\lambda(k^2)<0$ then a disturbance of wave vector $\mathbf{k}$ will decay with time. If $\lambda(k^2)>0$ for some k^2 then the disturbance with these wavenumbers will grow and the system will evolve to a non-uniform spatially structured solution. Typical dispersion curves are illustrated in Fig. 1.

On a two-dimensional domain we consider the wave vector $\mathbf{k}=(k_x, k_y)$ where $k_x = m\pi/L_x$, $k_y = l\pi/L_y$, where m and l are integers. These come from the zero flux boundary conditions and the linear eigenfunctions $\cos m\pi x/L_x \cos l\pi y/L_y$. Therefore on a rectangular domain the values of k^2 which produce a pattern are those where $\lambda(k^2)>0$ where

$$\mathbf{k}\cdot\mathbf{k} = k^2 = \pi^2\left(\frac{m^2}{L_x^2} + \frac{l^2}{L_y^2}\right). \tag{A4}$$

We can choose parameters D, α, s, r and N to isolate only one unstable wave vector. This mode selection (see Fig. 1) is simply a way of forcing a particular pattern to grow. The wave vector for the isolated mode occurs when $\lambda(k^2)=0$, that is when k satisfies

$$Dk^4 + \left[rNs + Ds - \frac{sN\alpha}{(1+N)^2}\right]k^2 + rNs^2 = 0. \tag{A5a}$$

We require equation (A5a) to have only one solution for k^2, so we further impose the condition for equal roots, namely

$$\left[rNs + Ds - \frac{sN\alpha}{(1+N)^2}\right]^2 - 4DrNs^2 = 0. \tag{A5b}$$

Hence the modulus of the critical wave vector is given by

$$k_c^2 = s\left(\frac{rN}{D}\right)^{1/2}. \tag{A5c}$$

By choosing D, s, r and N appropriately, we can find a k^2 from equation (A4) which satisfies equation (A5c), and then solve equation (A5b) for α (we take the larger root for α, so that k_c^2 is positive). This determines the point in (N, D, r, s, α) parameter space where mode (A5c) is isolated.

Note that if we decrease r or N, the critical wavenumber decreases, thus the spacing of the pattern increases, or if decreased enough, the pattern disappears altogether. This is a prediction of the model which could be tested experimentally as discussed in Section 4.

LITERATURE

Alberch, P. and E. A. Gale. 1983. Size dependence during the development of the amphibian foot. *J. Embryol. exp. Morph.* **76**, 177–197.

Bagnara, J. T. and M. E. Hadley. 1973. *Chromatophores and Color Change: The Comparative Physiology of Animal Pigmentation.* Englewood Cliffs, NJ: Prentice-Hall.

Bard, J. B. L. 1981. A model for generating aspects of zebra and other mammalian coat patterns. *J. theor. Biol.* **93**, 363–385.

Cocho, G., R. Perez-Pascual and J. L. Rius. 1987a. Discrete systems, cell–cell interactions and color pattern of animals. I. Conflicting dynamics and pattern formation. *J. theor. Biol.* **125**, 419–435.

Cocho, G., R. Perez-Pascual, J. L. Rius and F. Soto. 1987b. Discrete systems, cell–cell interactions and color patterns of animals. II. Clonal theory and cellular automata. *J. theor. Biol.* **125**, 437–447.

Ermentrout, B., J. Campbell and G. F. Oster. 1986. A model for shell patterns based on neural activity. *The Veliger* **28**, 369–388.

French, V., P. Bryant and S. Bryant. 1976. Pattern regulation in epimorphic fields. *Science*, N.Y. **193**, 969–981.

Grindod, P., S. Sinha and J. D. Murray. 1989. Steady state spatial patterns in a cell–chemotaxis model. *I.M.A. J. math. appl. Med. Biol.* **6**, 69–79.

Keller, E. F. and L. A. Segel. 1970. Initiation of slime mold aggregation viewed as instability. *J. theor. Bol.* **26**, 399–415.

Le Douarin, N. M. 1982. *The Neural Crest.* Cambridge: Cambridge University Press.

Mayer, T. C. 1980. The relationship between cell division and melanocyte differentiation in epidermal cultures from mouse embryos. *Dev. Biol.* **79**, 419–427.

Meinhardt, H. 1982. *Models of Biological Pattern Formation.* London: Academic Press.

Murray, J. D. 1979. A pattern formation mechanism and its application to mammalian coat markings. *Vito Volterra Symposium on Mathematical Models in Biology*, Accademia dei Lincei, Rome (Dec. 1979). Lecture Notes in Biomathematics, Vol. 39, pp. 360–399. Heidelberg: Springer Verlag.

Murray, J. D. 1981a. A pre-pattern formation mechanism for animal coat markings. *J. theor. Biol.* **88**, 161–199.

Murray, J. D. 1981b. On pattern formation mechanisms for lepidopteran wing patterns and mammalian coat markings. *Phil. Trans. R. Soc. Lond.* **B295**, 473–496.

Murray, J. D. 1988. Modelling the pattern formation mechanism in the formation of stripes on

alligators. In: *Proc. IXth International Congress on Mathematical Physics*, Swansea (July 1988), pp. 208–213. Bristol: Adam Hilger.

Murray, J. D. 1989. *Mathematical Biology*. Heidelberg: Springer-Verlag.

Murray, J. D., P. K. Maini and R. T. Tranquillo. 1988. Mechanochemical models for generating biological pattern and form in development. *Phys. Rep.* **171**, 59–84.

Murray, J. D., D. C. Deeming and M. J. W. Ferguson. 1990. Size dependent pigmentation pattern formation in embryos of *Alligator mississipiensis*: time of initiation of pattern formation mechanism. *Proc. R. Soc. Lond. B* **239**, 279–293.

Murray, J. D. and M. R. Myerscough. 1990. Pigmentation pattern formation on snakes. *J. theor. Biol.* (in press).

Newell, P. C. 1983. Attraction and adhesion in the slime mold *Dictyostelium*. In: *Fungal Differentiation: A Contemporary Synthesis*, J. E. Smith (Ed.), Mycology Series, Vol. 43, pp. 43–71. New York: Marcel Dekker.

Oster, G. F. and J. D. Murray. 1989. Pattern formation models and developmental constraints. *J. exp. Zool.* **251**, 186–202.

Oster, G. F., J. D. Murray, N. Shubin and P. Alberch. 1988. Evolution and morphogenetic rules. The shape of the vertebrate limb in ontogeny and phylogeny. *Evolution* **42**, 862–884.

Trinkaus, J. P. 1984. *Cells into Organs: The Forces that Shape the Embryo*. Englewood Cliffs, NJ: Prentice-Hall.

Turing, A. M. 1952. The chemical basis of morphogenesis. *Phil. Trans. R. Soc. Lond.* **B237**, 37–72.

Winters, K. H. 1985. *ENTWIFE User Manual* (Release 1). AERE-R 11577.

Winters, K. H. 1987. A bifurcation study of laminar flow in a curved tube of rectangular cross-section. *J. Fluid Mech.* **180**, 343–369.

Winters, K. H., M. R. Myerscough, P. K. Maini and J. D. Murray. 1991. Tracking bifurcating solutions of a model biological pattern generator. *Impact of Computing in Science and Engineering* (in press).

Wolpert, L. 1969. Positional information and the spatial pattern of cellular differentiation. *J. theor. Biol.* **25**, 1–47,

Wolpert, L. 1981. Positional information and pattern formation. *Phil. Trans. R. Soc. Lond.* **B295**, 441–450.